EUROPEAN ORGANIZATION FOR NUCLEAR RESEARCH

CERN-SPSC-2012-
SPSC-P-284 Add. 6
January 5, 2012

SEARCH FOR LONG-LIVED STATES OF $\pi^+\pi^-$ ATOMS

Addendum to the DIRAC Proposal

B.Adeva[n], L.Afanasyev[k], A.Anania[f], S.Aogaki[h], K.Augsten[b], P.Batyuk[k], A.Benelli[k], V.Brekhovskikh[m], T.Cechak[b], M.Chiba[i], C.Ciortea[j], C.Curceanu[e], P.Doškářová[b], A.Dudarev[k], D.Dumitriu[j], D.Drijard[a], D.Fluerasu[j], O.Gortchakov[k], K.Gritsay[k], C.Guaraldo[e], M.Gugiu[j] M.Hansroul[a], R.Hosek[b], Z.Hons[d], Y.Iwashita[h], V.Karpukhin[k], J.Kluson̆[b], M.Kobayashi[g], V.Kruglov[k], L.Kruglova[k], A.Kulikov[k], E.Kulish[k], A.Kuptsov[k], A.Lamberto[f], R.Lednicky[c], J.Martinčik[b], L.Nemenov[k], M.Nikitin[k], K.Okada[h], M.Pentia[j], M.Plo[n], P.Prusa[b], G.F.Rappazzo[f], A.Ryazantsev[m], A.Romero Vidal[e], V.Ronzhin[m], V.Rykalin[m], J.Saborido[n], J.Schacher[o], P.Shlyapnikov[m], J.Smolík[b], F.Takeutchi[h], T.Trojek[b] T.Urban[b] T.Vrba[b] P.Vázquez[n], V.Yazkov[l], Y.Yoshimura[g], M.Zhabitsky[k], P.Zrelov[k]

[a] CERN, Geneva, Switzerland
[b] Czech Technical University, Prague, Czech Republic
[c] Institute of Physics ASCR, Prague, Czech Republic
[d] Nuclear Physics Institute ASCR, Rez, Czech Republic
[e] INFN - Laboratori Nazionali di Frascati, Frascati, Italy
[f] Messina University and INFN-Messina, Italy
[g] KEK, Tsukuba, Japan
[h] Kyoto Sangyou University, Japan
[i] Tokyo Metropolitan University, Japan
[j] National Institute for Physics and Nuclear Engineering IFIN-HH, Bucharest, Romania
[k] JINR Dubna, Russia
[l] Skobeltsyn Institute for Nuclear Physics of Moscow State University
[m] IHEP Protvino, Russia
[n] Santiago de Compostela University, Spain
[o] Bern University, Switzerland

GENEVA
2011

Abstract

The proposed experiment is a further development of the DIRAC experiment already running at CERN PS. The observation of long-lived (metastable) states of $\pi^+\pi^-$ atoms ($A_{2\pi}$) will be performed with the same setup. This observation opens a possibility to measure the energy difference between ns and np states and to determine the value of the combination $2a_0 + a_2$ of S-wave $\pi\pi$ scattering lengths in a model-independent way. In combination with the $A_{2\pi}$ lifetime measurement providing the value $|a_0 - a_2|$ DIRAC is in the position to get a_0 and a_2 separately on the basis of $A_{2\pi}$ data only.

Contents

1 Physics motivation

The decay probability of $\pi^+\pi^-$ atoms ($A_{2\pi}$) is dominated by the annihilation process

$$\pi^+ + \pi^- \to \pi^0 + \pi^0 \tag{1}$$

(branching ratio ~ 99.6%) and depends on the difference between the s-wave $\pi\pi$ scattering lengths with isospins zero (a_0) and two (a_2) [29, 6, 20, 19].

$$\frac{1}{\tau} \approx W_{\pi^0\pi^0} = R\,|a_0 - a_2|^2 . \tag{2}$$

The most accurate ratio of $W_{\pi^0\pi^0}$ to the square of $\pi\pi$ scattering length difference $|a_0 - a_2|$ was derived in [17]: R has been obtained within 1.2% accuracy.

In order to get values of a_0 and a_2 separately from $\pi^+\pi^-$ atom data, one may exploit the fact that the energy splitting between the levels ns and np, $\Delta E_n = E_{ns} - E_{np}$, depends on another combination of the scattering lengths: $2a_0 + a_2$ [14]. In the πN case, this dependence of the atomic level shift on scattering lengths in the s-states has been derived in [11]. The influence of the strong and electromagnetic interactions on the $A_{2\pi}$ energy structure was studied in [21, 5, 14, 16, 15]. An elaborated analysis of the $A_{2\pi}$ energy structure was performed in [28].

The energy shift for the levels with the principal quantum number n and orbital quantum number l includes few contributions:

$$\Delta E_{nl} = \Delta E^{\rm em}_{nl} + \Delta E^{\rm vac}_{nl} + \Delta E^{\rm str}_{nl}, \tag{3}$$

where $\Delta E^{\rm em}_{nl}$ includes relativistic insertions, finite-size effect, self-energy corrections due to transverse photons and transverse photon exchange. The term $\Delta E^{\rm vac}_{nl}$ includes the contributions from the vacuum polarization. The last term $\Delta E^{\rm str}_{nl}$ takes into account strong interaction effects and is related to the $\pi\pi$ scattering lengths as follows:

$$\Delta E^{\rm str}_{n0} = A_n(2a_0 + a_2). \tag{4}$$

For the ground state, the coefficient A_1 is known within 2.1% [28]. The values of the energy shifts for the levels with $n = 1$ and 2 are presented in Table 1.

Table 1: *Numerical values for the energy shift [28].*

	$\Delta E^{\rm em}_{nl}$(eV)	$\Delta E^{\rm vac}_{nl}$(eV)	$\Delta E^{\rm str}_{nl}$(eV)
$n=1,\ l=0$	-0.065	-0.942	$-3.80 \pm .1$
$n=2,\ l=0$	-0.012	-0.111	-0.47 ± 0.01
$n=2,\ l=1$	-0.004	-0.004	$\simeq -1\times 10^{-6}$

Hence, the theoretical value for the 2s − 2p energy splitting is given by

$$\Delta E^{\rm 2s-2p} = \Delta E^{\rm str}_{20} + \Delta E^{\rm em}_{20} - \Delta E^{\rm em}_{21} + \Delta E^{\rm vac}_{20} - \Delta E^{\rm vac}_{21} = -0.59 \pm 0.01{\rm eV}. \tag{5}$$

By measuring the value of $\Delta E_n = \Delta E^{n{\rm s}-n{\rm p}}$ one can determine the numerical value of $\Delta E^{\rm str}_{n0}$, as all other terms in Eq. (3) have been calculated with a high accuracy. From (5) and Table 1 it follows that the strong interaction effects contribute up to 80% of the full energy shift. This fact provides a high sensitivity of a $\Delta E^{\rm 2s-2p}$ measurement to the value of the term $2a_0 + a_2$. Thus, measurements of the energy shift ΔE_n make it possible to obtain values for the new combination of scattering lengths $2a_0 + a_2$ in a model-independent way.

The most accurate theoretical predictions for the s-wave $\pi\pi$ scattering lengths have been achieved by [8] (in units $M^{-1}_{\pi^+}$):

$$a_0 = 0.220 \pm 2.3\%\,, \quad a_2 = -0.0444 \pm 2.3\%\,, \quad a_0 - a_2 = 0.265 \pm 1.5\%\,. \tag{6}$$

The best experimental results obtained by NA48/2 from investigating the K_{e4} decay [24] are the following ones:

$$\begin{aligned} a_0 &= 0.2220 \pm 0.0128_{\text{stat}} \pm 0.0050_{\text{syst}} \pm 0.0037_{\text{theo}} \\ a_2 &= -0.0432 \pm 0.0086_{\text{stat}} \pm 0.0034\text{syst} \pm 0.0028_{\text{theo}} \end{aligned} \tag{7}$$

From the analysis of the decay $K^{\pm} \to \pi^{\pm}\pi^0\pi^0$ the same experiment obtained [23]

$$\begin{aligned} a_0 - a_2 &= 0.2571 \pm 0.0048_{\text{stat}} \pm 0.0025_{\text{syst}} \pm 0.0014_{\text{ext}} \\ a_2 &= -0.024 \pm 0.013_{\text{stat}} \pm 0.009\text{syst} \pm 0.002_{\text{ext}} \end{aligned} \tag{8}$$

There are also addional theorectical uncertainties of 0.0088 for $a_0 - a_2$ and of 0.015 for a_2.

The result of DIRAC based on 21000 "atomic pairs" collected in 2000–2003 [1] is

$$|a_0 - a_2| = 0.2533^{+0.0080}_{-0.0078}(\text{stat})^{+0.0077}_{-0.0072}(\text{sys}) = \ldots \pm 4.3\%_{\text{tot}}. \tag{9}$$

2 Study of long-lived states as a method for energy shift measurement

The method for measuring ΔE_n was qualitatively discussed in [27]. By studying the dependence of the $A_{2\pi}$ long-lived state ($l \geq 1$) lifetime on an applied electric field, it is possible to extract an experimental value for ΔE_n [27, 25, 26].

In inclusive processes, $A_{2\pi}$ are produced in s-states distributed over the principal quantum number n proportionally to n^{-3}. When moving inside the target, the relativistic $A_{2\pi}$ interacts with the electric field of the target atoms and, with some probability, will leave the target with orbital angular momentum $l > 0$. Calculations show that up to $\sim 10\%$ of the atoms, generated in a thin target, reach the vacuum region in a long-lived state [3]. The main part of these atoms will be in the 2p-state. For $A_{2\pi}$ in p-state the decay into two π^0-mesons is forbidden by the conservation law for the angular momentum, and the process $A_{2\pi} \to \pi^0 + \gamma$ is also strongly suppressed. Therefore, the main mechanism of the 2p-state decay is the 2p–1s radiative transition with a subsequent annihilation from the 1s-state into two π^0 with the lifetime of $\tau_{1s} \approx 3 \times 10^{-15}$ s. Thus, the lifetime of the atom in the 2p-state is determined by the radiative transition probability equivalent to $\tau_{2p} = 1.17 \times 10^{-11}$ s [27]. For the average $A_{2\pi}$ momentum in DIRAC of 4.5 GeV/c ($\gamma = 16.1$) the corresponding decay length is 5.7 cm for $2p$-state , 19 cm for $3p$ and 43 cm for $4p$.

The $A_{2\pi}$ decay from ns-states is allowed with the corresponding lifetimes $\tau_{ns} = \tau_{1s} n^3$. Since the lifetime in np-states is about 10^3 times larger than ns-state lifetime, it is possible to measure the energy difference of these levels by exerting an electrical field on the atom: the procedure is to track the field dependence of the decay probability, due to the mixing of ns- and np-states in the external electrical field.

In [25] the influence of constant magnetic field on the $A_{2\pi}$ atom lifetime has been studied and the possibility demonstrated to measure the $2s-2p$ energy splitting with the use of relativistic atomic beams.

The transverse magnetic lab field B_0 is increased to $B = \gamma B_0$ (γ is Lorentz factor) in amplitude in the atom reference frame. The corresponding electric field has nearly the same amplitude $F = \beta B$ (β is the atom velocity in the lab frame) and is perpendicular to the atom momentum. In the electric field a small admixture of the $2s$-state to the $2p$-state wave function arises. This admixture may cause a significantly faster decay for atoms initially being in the $2p$-state. For the case of $B_0 = 4$ T and $\gamma = 20$, the decay rate increases more than twice.

Another possibility to measure the energy shift ΔE_n is the resonance method [26] which allows to achieve a higher accuracy.

Similar approach can be applied to measure energy shifts in $\pi^{\pm}K^{\mp}$ atoms. The energy difference between the $2s$ and $2p$ πK-atomic levels consists of two electromagnetic components, $\Delta E^{em}_{2s-2p} = -0.013$ eV and $\Delta E^{vac}_{2s-2p} = -0.27$ eV, and a strong component, $\Delta E^{\rm str}_{2s-2p} \propto (2a_0^{1/2} + a_0^{3/2})$ (see ref. [28]). By inserting the πK scattering lengths from [7] in the above equation, one gets $\Delta E^{\rm str}_{2s-2p} = (-1.1 \pm 0.1)$ eV [28], yielding in total the $2{\rm s}-2{\rm p}$ energy splitting $\Delta E^{2{\rm s}-2{\rm p}} = -1.4 \pm 0.1$ eV. The strong part $\Delta E^{\rm str}_{2s-2p}$ of this splitting is - in principle - measurable [27]. The quantity $2a_0^{1/2} + a_0^{3/2}$ as described in Chiral Perturbation Theory (ChPT) involves a combination of low energy constants, $2L_6 + L_8$, which provides information on the quark condensate and the strange to non-strange quark mass ratio [9].

3 Generation of $A_{2\pi}$ in long-lived states on Beryllium

Up to now DIRAC (see Fig. 1) took data with a Nickel target of 100 μm thickness providing the best sensitivity to the $A_{2\pi}$ lifetime. To get the maximum yield of the long-lived states the thickness of Ni target needs to be reduced to 5 μm, that requires an increase in the beam intensity of a factor 20 in order to obtain the same number of proton-target interactions. However this cannot be realized for a variety of reasons: accelerator limits, radio-protection restrictions, overloading a major part of detectors and so on. For this reason the target material need to be replaced by one having a higher nuclear efficiency.

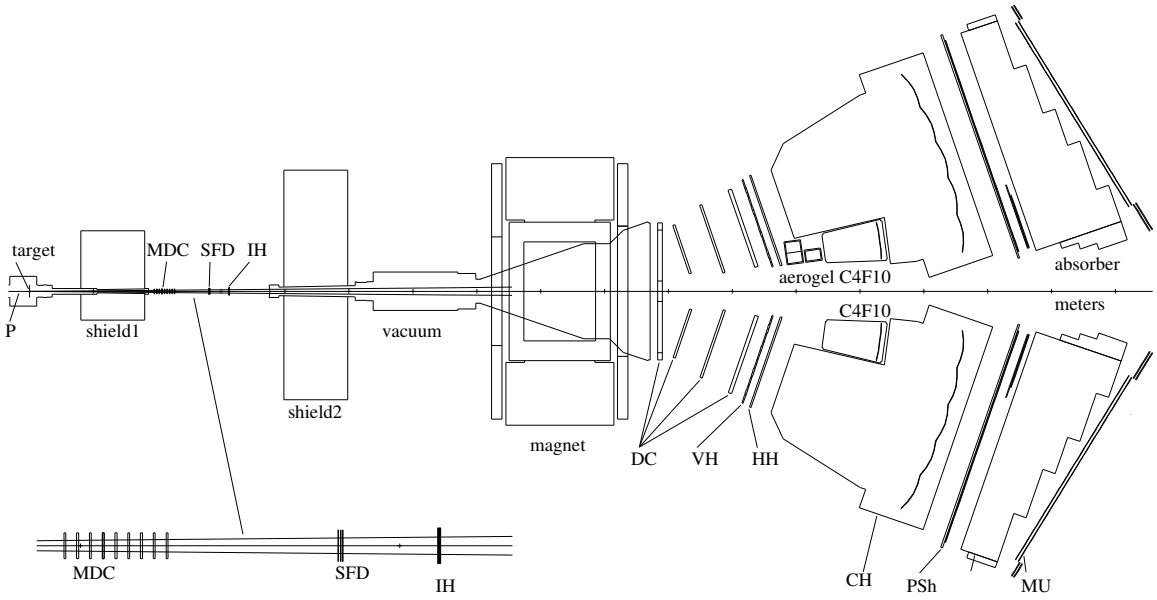

Figure 1: *DIRAC setup: MDC are microdrift gas chambers, SFD is a scintillating fiber detector and IH is a scintillation ionization hodoscope. Downstream the spectrometer magnet there are drift chambers (DC), vertical (VH) and horizontal (HH) scintillation hodoscopes, Cherenkov detectors containing nitrogen (CH), heavy gas C4F10 and aerogel radiators, shower detectors (PSh) and scintillation muon detectors (MU).*

For a 100 μm Beryllium target the nuclear efficiency ε_{nucl} is 7 times larger than for 5 μm Ni (see Table 2). Therefore the proton beam intensity must be only about 3 times larger in order to get the needed number of primary interactions.

The proton-target interaction will generate $A_{2\pi}$ in ns states as follows:

$$W_{1s} = 83\%, W_{2s} = 10.4\%, W_{3s} = 3.1\%, W_{>3s} = 3.5\%.$$

Passing through the target, a fraction of $A_{2\pi}$ interacts with Be-atoms and hence will be excited into $2p, 3p, 4p, ...$ states (see Fig. 2). The main excitation processes are $1s \to np$ transitions.

Table 2: *Targets thickness L in micron, in radiation length (X/X_0) and nuclear efficiency (probability for proton-nucleus interaction).*

Target	L μm	$\frac{X}{X_0} \times 10^4$	$\varepsilon_{nucl} \times 10^4$
Be	100	2.84	2.45
Ni	5	3.53	0.34

To obtain numerical values for the $A_{2\pi}$ long-lived state production we chose the approach in which the evolution of the atomic state population is described in terms of probabilities [3],[4]. The values below were averaged over the experimental $A_{2\pi}$ lab momentum distribution and the $A_{2\pi}$ ground-state lifetime has been fixed to 3.0×10^{-15} s

After the investigating several Be target thicknesses the optimal one has been found to be 100 μm [10]. The distribution of long-lived $A_{2\pi}$ at the Be target exit over quantum number n and orbital momentum l is presented in Table 3. The total number of long-lived $A_{2\pi}$ is 6 % of the total number of $A_{2\pi}$ generated in Be target.

Table 3: *Relative populations (‰) of $A_{2\pi}$ long-lived states at the Be target exit as a function of principal quantum number n and orbital momentum l.*

l \ n	2	3	4	5	6	7	8
1	417	148	48	18	7	3	1
2	0	117	49	20	9	4	1
3	0	0	45	21	10	4	2
4	0	0	0	20	10	5	2
5	0	0	0	0	10	5	2
6	0	0	0	0	0	4	2
7	0	0	0	0	0	0	2

Long-lived atoms annihilate at a distance more than a few cm, while the short-lived states annihilate in the target or near the target at a distance of less than 2 mm (Fig. 2). The decay lengths of $A_{2\pi}$ with $\gamma = 20$ in $1s, 2s, 3s$ and $4s$ states are 0.017 mm, 0.14 mm, 0.46 mm and 1.1 mm. About 6.3% of the $A_{2\pi}$ atoms break up in the target, producing $n_{\rm A}^{\rm Be}$ atomic pairs having $Q_T \leq 1.5$ MeV/c. (Here and below Q_T and Q_L are the transverse and longitudinal component of the relative momentum Q in the atomic pair c.m.s. correspondingly.)

The proton beam interacting with the target can produce also Coulomb ($N_{\rm C}^{\rm Be}$) and non-Coulomb pairs ($N_{\rm nC}^{\rm Be}$). These pairs are detected by the setup and represent the main background.

By analyzing experimental distributions of $\pi^+\pi^-$ pairs in Q_T and Q_L one can obtain the amount of Coulomb and non-Coulomb pairs. The number of Coulomb pairs with small Q ($Q \leq 3$ MeV/c) allows one to calculate the number of produced atoms $N_{\rm A}$, using precise ($\leq 1\%$) formula and the expected number of atomic pairs $n_{\rm A}^{\rm Be}$ (see for example [2]).

Knowing the $A_{2\pi}$ ground state lifetime, the theory of $A_{2\pi}$ interaction with tarteg atoms and the description of their propagation through the target (precision $\leq 1\%$) allow to calculate the number of $A_{2\pi}$ in long-lived states produced in Be $N_{\rm A}^l(Be)$, the number of atomic pairs $n_{\rm A}^{\rm Be}$ and the corresponding distributions in Q, Q_T and Q_L. The value $n_{\rm A}^{\rm Be}$ can also be extracted from the experiment by subtracting the Coulomb and non-Coulomb pair background.

4 Detection of $A_{2\pi}$ in long-lived states with a thin Platinum foil

Placing a 2 μm thin Pt foil downstream the Be target [10], the largest part of long-lived atoms, $N_{\rm A}^{l}$, will break up, providing an additional number of atomic pairs, $n_{\rm A}^{l}$ (see Fig. 2). Table 4 presents the atom breakup probability as a function of foil thickness and $A_{2\pi}$ quantum numbers.

Table 4: *Breakup probability of $A_{2\pi}$ in np states for different thicknesses of Platinum foils ($A_{2\pi}$ momentum $P_{\rm A} = 4.5\,GeV/c$ and $A_{2\pi}$ ground-state lifetime $\tau = 3\times10^{-15}\,s$).*

Thickness (μm)	2p	3p	4p	5p	6p	7p
0.1	0.0251	0.0520	0.0858	0.1327	0.2035	0.3219
0.2	0.0559	0.1175	0.1978	0.3001	0.4185	0.5392
0.5	0.1784	0.3595	0.5537	0.7176	0.8323	0.9043
1.0	0.4147	0.6895	0.8553	0.9324	0.9667	0.9828
1.5	0.6084	0.8526	0.9446	0.9765	0.9889	0.9944
2.0	0.7422	0.9244	0.9743	0.9895	0.9951	0.9975
3.0	0.8844	0.9739	0.9918	0.9967	0.9985	0.9992

For the Pt thickness of 2 μm, the breaking probability of long-lived $A_{2\pi}$ averaged over populations is 0.94. About 95% of the atomic pairs have $0 \le Q_T \le 1$. MeV/c. If the foil were thicker, then the upper limit of Q_T would increase that would increase the number of background Coulomb pairs and hence the precision for a $n_{\rm A}^{l}$ measurement decreases. So there is no reason to use the foil thicker than 2 μm.

Atoms $A_{2\pi}$ in p states in the region between the Be and Pt can deexcite radiatively into s states with subsequent annihilation (Fig. 3).

The lifetimes of np states and their lab decay lengths λ for $A_{2\pi}$ average Lorentz factor $\gamma = 16$ are presented in Table 5. The distance between the Be target and the Pt foil has been chosen to be 100 mm to exclude interactions of the primary beam halo with the Pt foil.

Table 5: *Lifetimes τ from np states and their lab decay lengths λ in for $\gamma = 16$.*

state	$\tau\cdot10^{11}s$	λ [cm]
2p	1.17	5.7
3p	3.94	19
4p	9.05	44
5p	17.5	84.5
6p	29.9	144
7p	46.8	226
8p	69.3	335

5 Measurement of $A_{2\pi}$ production rate in p-Be interactions in 2010 and 2011

During 7.5 days in August 2010 a small data sample was collected with 100 μm Beryllium target at the intensity $2.6\cdot10^{11}$ proton per spill. This intensity was chosen to provide the same number of

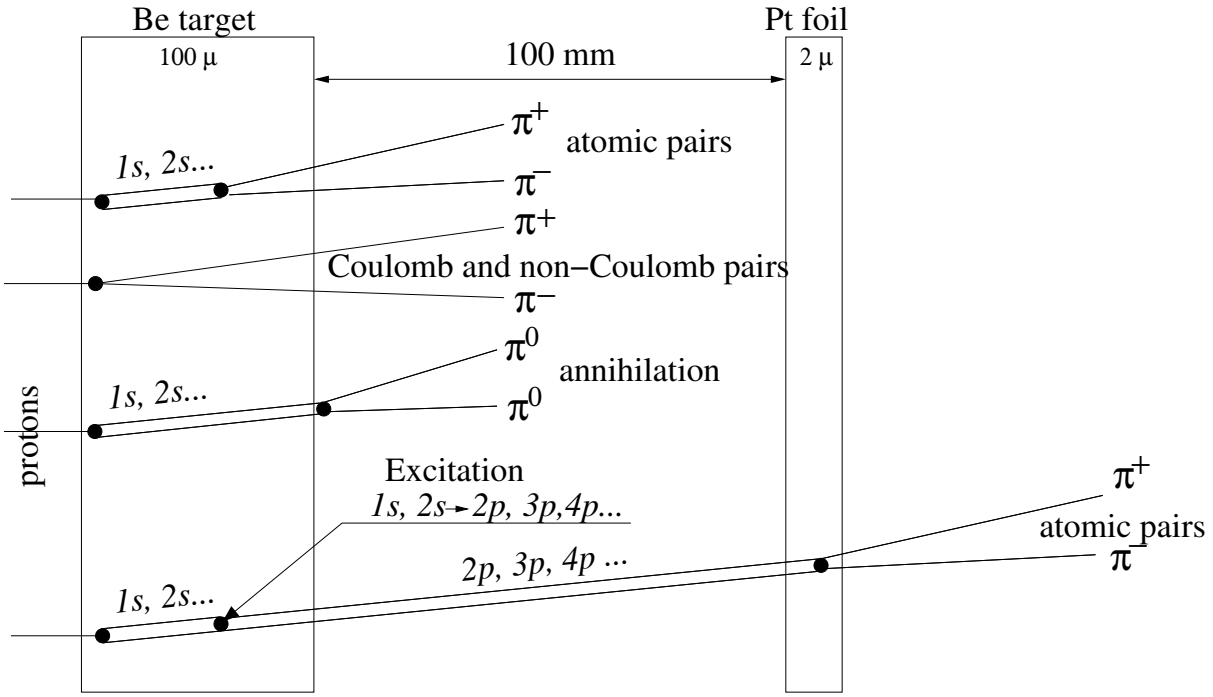

Figure 2: *Method to observe long-lived $A_{2\pi}$ by means of a breakup foil (Pt).*

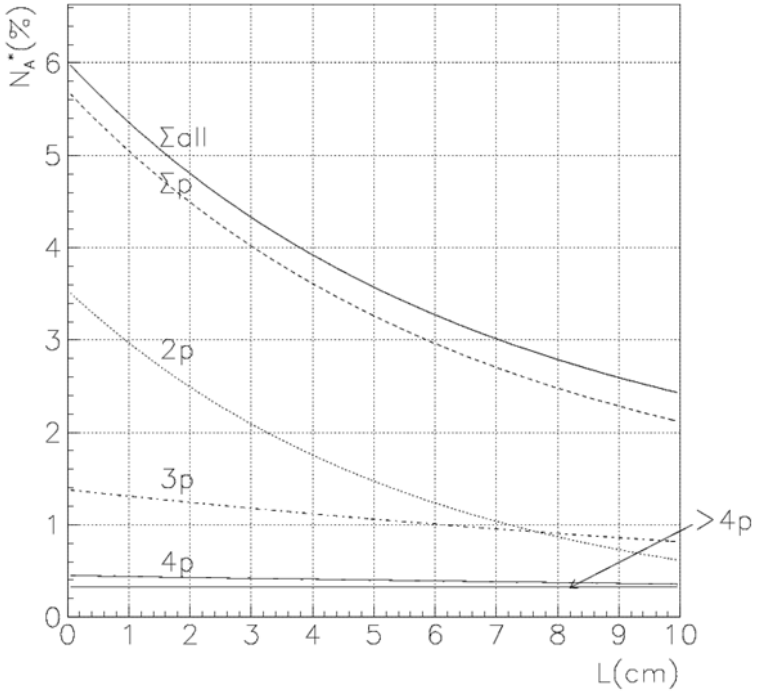

Figure 3: *Part of atoms created in the Be target and then broken up in the Pt foil versus the distance between the target and foil (L) for all metastable states with $n > 1, l > 0$ (Σall), for sum of np states (Σp) and for some individual p states. The foil thickness is 2 μm.*

primary interactions in the target as in the usual working condition for DIRAC during 2010, with the 100 μm Ni target and a $9.5 \cdot 10^{10}$ proton per spill intensity. The total spill number was $53 \cdot 10^3$ and the proton flux through the target was $1.4 \cdot 10^{16}$. The measured multiplicity with Be in all detectors differs from the ordinary one by 2–3%. The single detector counts increased in different proportions for the specific detectors: Ionization Hodoscope — 8%; Vertical Hodoscope positive arm — 3%, negative arm — 17%; Cherenkov counter for positrons — 25%, for electrons — 30%; Cherenkov counter for pions — 7% for both arms. The number of the first level triggers increased by 5%.

These data were analyzed in order to find the number of generated atoms using the standard analysis procedure for the DIRAC experiment [2]. There is a possibility to increase the efficiency of event reconstruction by a factor 1.2–1.5. Fig. 4 presents the distribution of experimental data (points with error bars) over the absolute value of Q_L for the events with $Q_T < 1$ MeV/c. The dashed line represents the fit of the experimental data with the sum of simulated "Coulomb" and "non Coulomb" pair distribution (see section 6) in the range $|Q_L| > 1$ MeV/c that eliminates the contribution of atomic pairs. The only free parameter in the fit is the fraction of "Coulomb pairs" with respect to "non-Coulomb" pairs, resulting in 0.18. Using the known ratio of cross sections between $A_{2\pi}$ and "Coulomb pairs" [27] and the experimentally measured number of Coulomb pairs, the number of generated atoms for the observed spill number of $53 \cdot 10^3$ has been estimated:

$$N_A = 736 \pm 75 \tag{10}$$

The same measurement was repeated in the beginning of the run in 2011 with proton beam intensity $3 \cdot 10^{11}$ p/spill, number of spills 24271 and total proton flux through the target $6.2 \cdot 10^{15}$. The distribution of prompt $\pi^+\pi^-$ pairs is presented in Fig. 5. From the analysis of this distribution, the number of generated $A_{2\pi}$ has been estimated to be:

$$N_A = 368 \pm 32 \tag{11}$$

which coincides after normalisation to the same proton flux with the result obtained in 2010. In 2011 the total spill numbers was $7.5 \cdot 10^5$. In accordance with 2010 and 2011 measurements for the expected number of spills of 10^6 in 2012 the total number of generated $A_{2\pi}$ will be on the level 14000-15000.

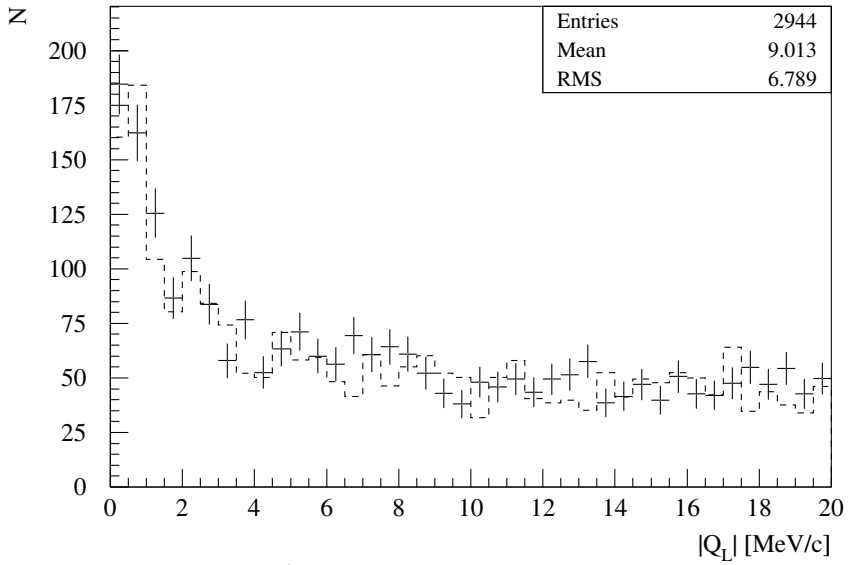

Figure 4: *Distribution over $|Q_L|$ of $\pi^+\pi^-$ pairs collected in 2010 with Beryllium target with the cut $Q_T < 1$ MeV/c. Experimental data (points with error bars) have been fitted by a sum of the simulated distribution of "Coulomb" and "non-Coulomb" pairs (dashed line).*

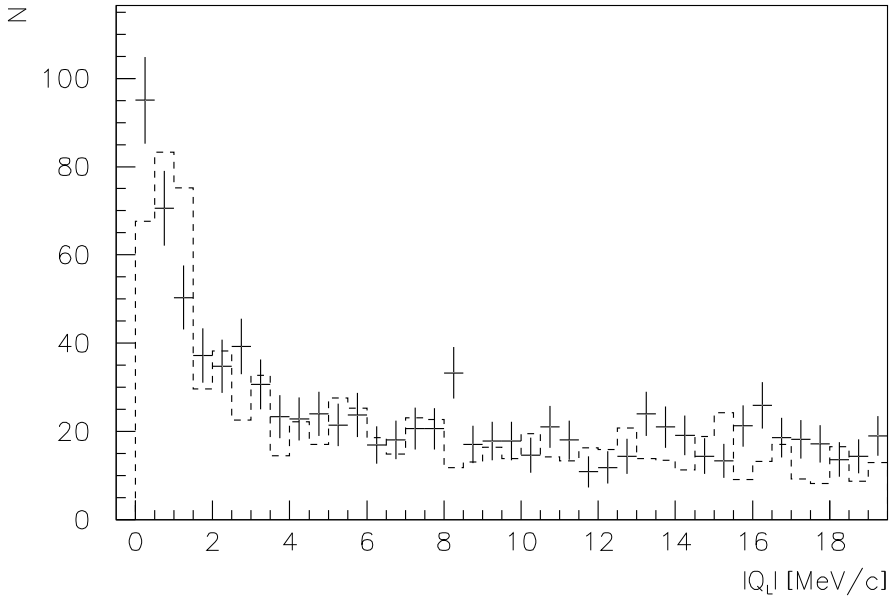

Figure 5: *Distribution over $|Q_L|$ of $\pi^+\pi^-$ pairs collected in 2011 with Beryllium target with the cut $Q_T < 1$ MeV/c. Experimental data (points with error bars) have been fitted by a sum of the simulated distribution of "Coulomb" and "non-Coulomb" pairs (dashed line).*

6 Simulation of all $\pi^+\pi^-$ pair distributions at experimental conditions

For the simulation of $\pi^+\pi^-$ pairs (atomic pairs, Coulomb and non-Coulomb pairs) the DIPGEN generator [30] was used with modifications describing interaction of the long-lived atoms with the additional Platinum foil. For the long-lived atoms the following processes were considered: their production in the Beryllium target, their decay in the region before the Platinum foil and breakup in the foil producing atomic pairs.

In Table 6 the relative populations of $A_{2\pi}$ long-lived states at the foil entry are given. In Table 7, the numbers of atomic pairs produced in the 2 μm Pt foil from states with specific n and l numbers are given. All numbers are normalized to the sum over each table and given in ‰.

Table 6: *Relative populations (in ‰) of $A_{2\pi}$ long-lived states at the foil entry.*

l \ n	2	3	4	5	6	7	8
1	114	150	69	30	12	6	2
2	0	176	86	37	17	7	3
3	0	0	84	41	19	9	3
4	0	0	0	40	19	9	4
5	0	0	0	0	19	9	4
6	0	0	0	0	0	9	4
7	0	0	0	0	0	0	4

Table 7: *The relative numbers (in ‰) of atomic pairs produced in the 2 μm Pt foil from states* (n,l).

l \ n	2	3	4	5	6	7	8
1	56	82	53	29	17	9	4
2	0	95	73	46	28	15	7
3	0	0	78	54	35	21	10
4	0	0	0	59	37	24	13
5	0	0	0	0	43	27	14
6	0	0	0	0	0	28	15
7	0	0	0	0	0	0	15

Then the pairs generated by the DIPGEN were transferred into GEANT-DIRAC (setup simulator) and ARIANE (reconstruction tool) programs. The distributions of reconstructed values of Q_L and Q_T for 'non-Coulomb", "Coulomb pairs" and "atomic pairs" from metastable atoms are shown in Figs. 6 and 7.

In the case of a 100 mm target-foil distance the total breakup probability of metastable atoms in the 2 μm Pt foil is 0.94.

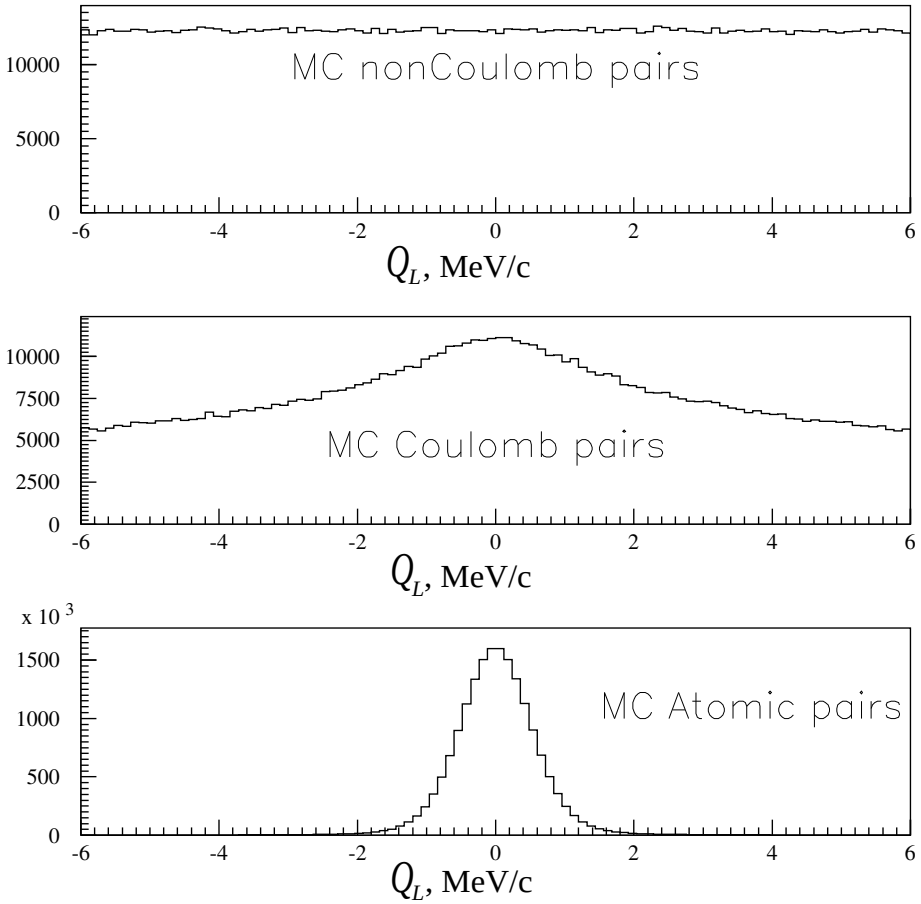

Figure 6: *Distributions of reconstructed values of* Q_L *for non-Coulomb, Coulomb pairs and pairs from metastable atom.*

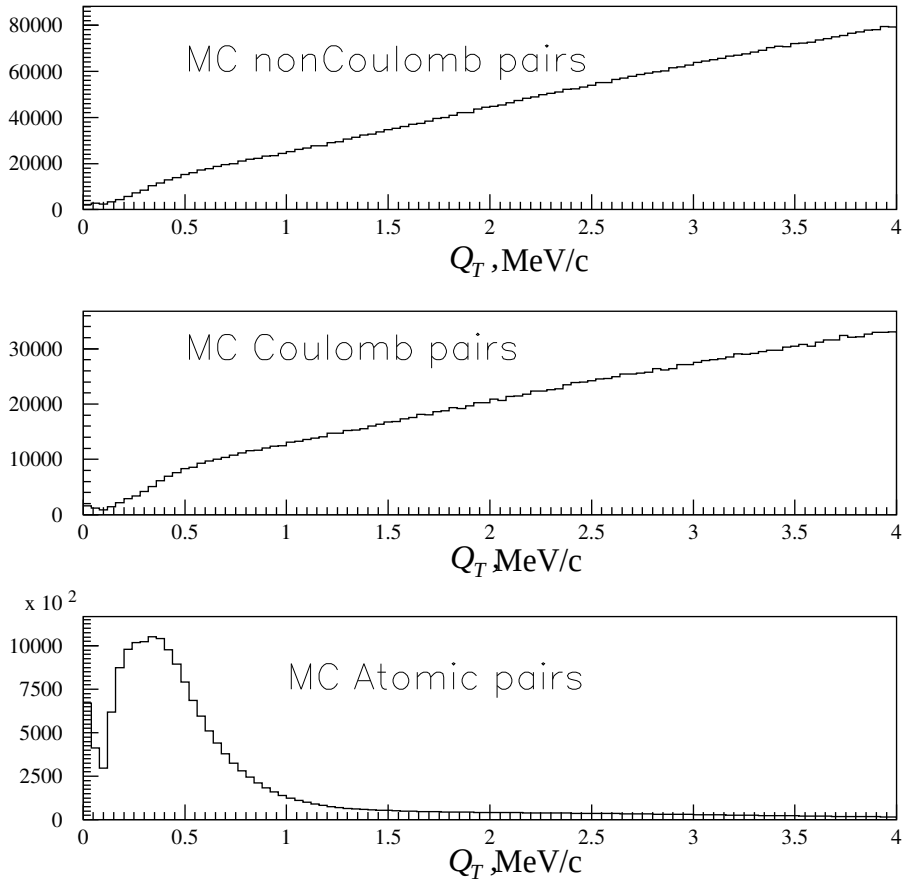

Figure 7: *Distributions of reconstructed values of Q_T for non-Coulomb, Coulomb pairs and pairs from metastable atom.*

7 Simulation of long-lived $A_{2\pi}$ observation

To evaluate the necessary running time for the observation of long-lived $A_{2\pi}$ the "experimental data" has been simulated as a sum of the following sets of data : "atomic pairs" from long-lived atoms produced in the Platinum foil, "atomic pairs", "Coulomb pairs", "non-Coulomb pairs" and accidentals from the Beryllium target . The total amount of data and the relative contribution of the different components are obtained from the analysis of the experimental data collected in 2010 with the Beryllium target (see section 5). Fig. 8 presents the distribution of simulated data over the Y (vertical) projection of the relative momentum Q . The cuts on $|Q_X| < 1$ MeV/c and $|Q_L| < 1$ MeV/c have been applied. The simulation shows that in each projection such criterion selects more than 90% of "atomic pairs" from long-lived atoms. Hatched area is the sum of all pairs produced in Beryllium target and light area corresponds to "atomic pairs" from long-lived atoms (broken in the Platinum foil). The signal-to-background ratio is small. It can be improved by installing an additional magnet which generates the horizontal magnetic field in the gap between Be target and Pt foil. A magnet with the bending power of 0.01 Tm would shift the Q_Y value by 6 MeV/c only for the pairs produced in the Be target, leaving unchanged the Q_Y distribution of the pairs produced in the Pt foil. A permanent magnet made of $Ne_2Fe_{14}B$ with such characteristics was used in the 2011 run.

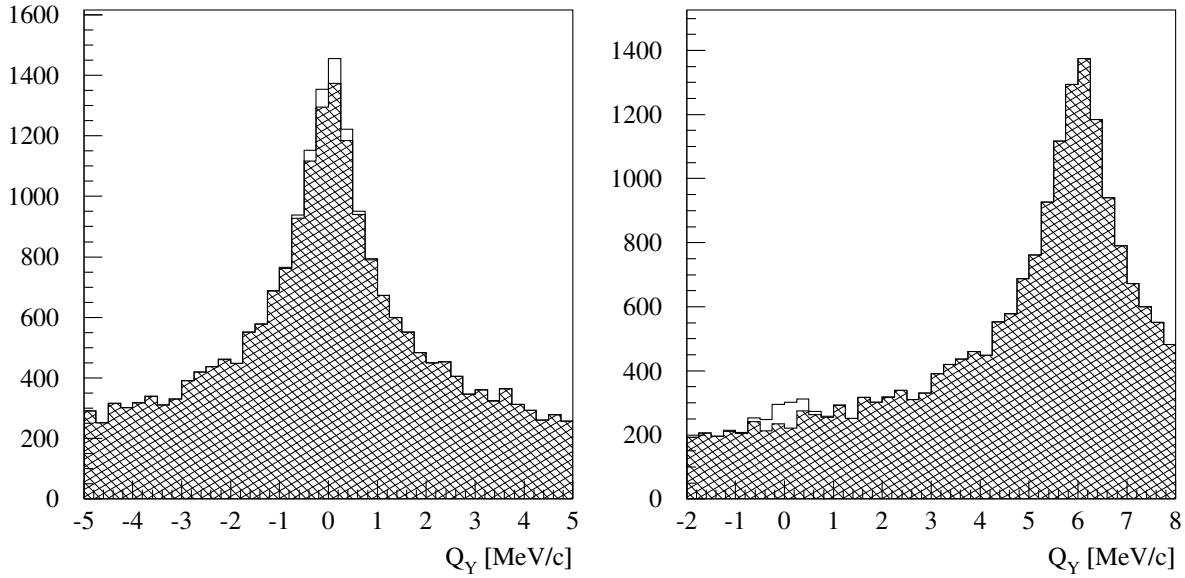

Figure 8: *Simulated distribution of $\pi^+\pi^-$ pairs over Q_Y with criteria: $|Q_X| < 1$ MeV/c, $|Q_L| < 1$ MeV/c. "Atomic pairs" from long-lived atoms (light area) above the background produced in Beryllium target (hatched area): in left side without the magnet and in right side with magnet used in 2011.*

A new sample of simulated data with the additional permanent magnet has been fitted with the sum of the distributions of atomic pairs from long-lived atoms, "Coulomb pairs" and "non-Coulomb pairs". The atomic pairs produced in the Be target with Q_Y about 6 MeV/c are absent in the fit region. The fitting procedure is the standard one used in DIRAC [2]. The free parameters in the fit are the amounts of each of the former distributions relative to the total number of events. The fit results for the distribution over Q_L (with cut $Q_T < 1$ MeV/c) are presented in Fig. 10. The number of atomic pairs is found to be:

$$n_A^l = 281 \pm 48$$

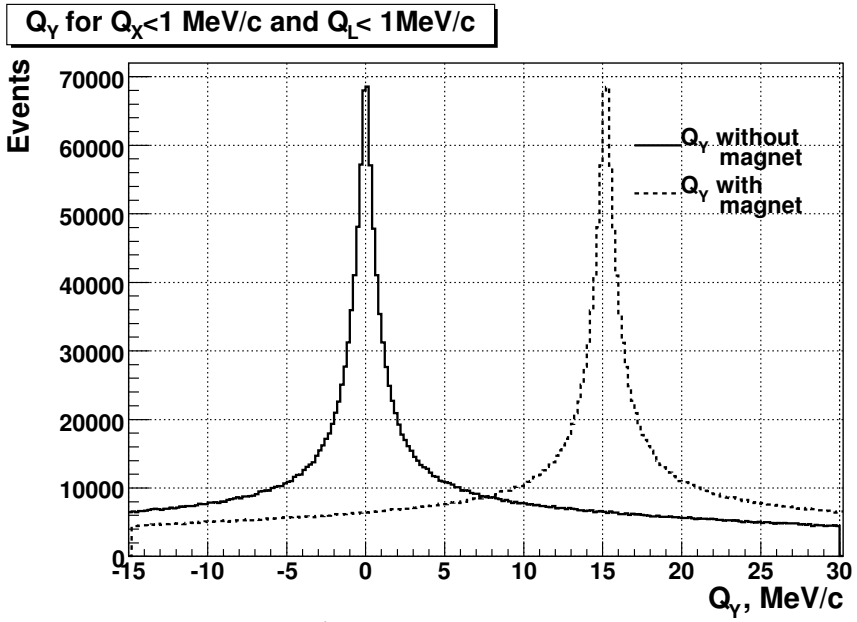

Figure 9: *Simulated distribution of $\pi^+\pi^-$ pairs over Q_Y with criteria: $|Q_X| < 1$ MeV/c, $|Q_L| < 1$ MeV/c produced in Beryllium target. The events without magnet (solid line) are distributed around 0 and events with the new magnet are shifted by 15 MeV/c (dashed line).*

Analysis of the experimental data accounting widths of the atomic pairs distribution over different components of the relative momentum Q allows to find the variable F which provides the distribution of atomic pairs with the best signal-to-background ratio:

$$F = \sqrt{\left(\frac{Q_X}{0.50}\right)^2 + \left(\frac{Q_Y}{0.32}\right)^2 + \left(\frac{Q_L}{0.56}\right)^2} \tag{12}$$

Here 0.50, 0.32 and 0.56, in units of MeV/c, are RMSs of the atomic pairs distribution over corresponding components of the relative momentum Q.

Fig. 11 presents results of analysis for distribution of $\pi^+\pi^-$ pairs over F. It provides a greater number of found atomic pairs due to the weaker cut on $Q_T < 2$ MeV/c and a better signal-to-error ratio:

$$n_A^l = 327 \pm 37 \tag{13}$$

$$\frac{n_A}{\sigma_{n_A}} = 8.8 \tag{14}$$

It is worth noting that the simulated number n_A^l is 310.

In order to justify an observation of long-lived $A_{2\pi}$ it is needed to achieve a ratio between the signal and error larger than 5. The current simulation provides the ratio of 8.8. This means that the confidence level to observe long-lived $A_{2\pi}$ will be close to 100%.

A new permanent magnet with the bending power of 0.023 Tm will be used in 2012 (see section 9). The simulated distribution of $\pi^+\pi^-$ pairs over Q_Y for this magnet is showen in Fig. 9. The expected background level will be smaller by a factor 1.5 and the signal-to-error ratio will be at the level large than 9.

In the approach without the additional magnet, the accuracy of signal separation would be worse. In equal conditions the simulated number of reconstructed atomic pairs is $n_A^l = 334 \pm 89$. To achieve the value of 5 in the signal-to-error ratio, required for the observation, the needed statistic should be increased by 1.8 that could be accomplished with a higher efficiency of the event reconstruction and/or a longer run time.

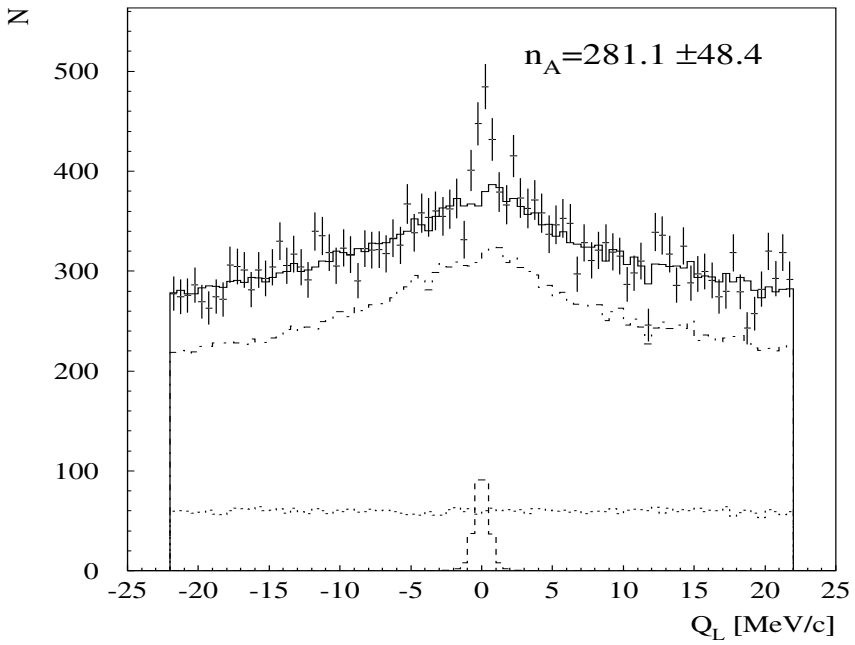

Figure 10: *Simulated distribution of $\pi^+\pi^-$ pairs over Q_L, with criterion Q_T < 1 MeV/c. "Experimental data" (points with error bars) are fitted by the sum of "atomic pairs" from long-lived states (dashed line), "Coulomb pairs" (by dotted-dashed line), "non-Coulomb pairs" (dotted line). The background sum is shown by the solid line.*

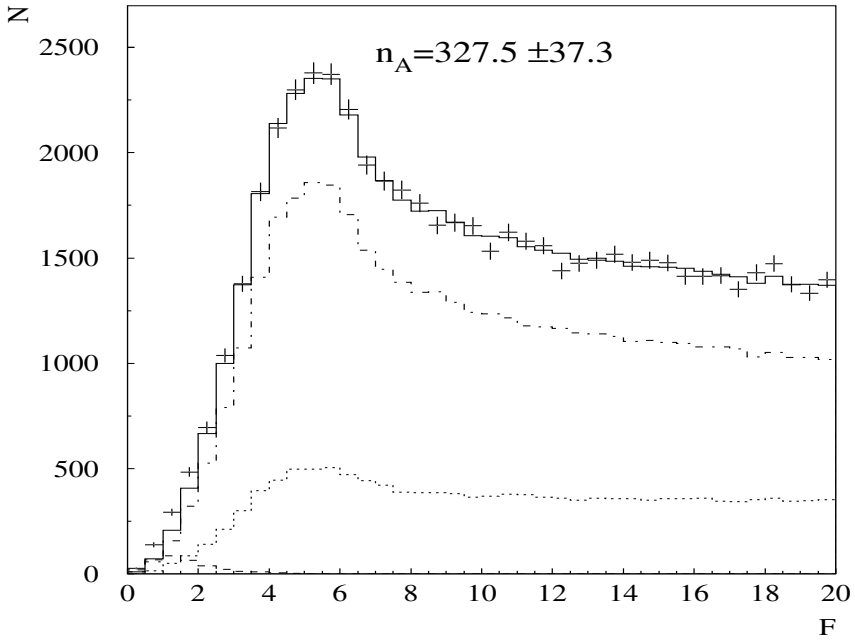

Figure 11: *Simulated distribution of $\pi^+\pi^-$ pairs over F, with criterion Q_T < 2 MeV/c. "Experimental data" (points with error bars) are fitted by the sum of "atomic pairs" from long-lived states (dashed line), "Coulomb pairs" (dotted-dashed line), "non-Coulomb pairs" (dotted line). The background sum is shown by the solid line.*

8 Permanent magnet degradation during 2011.

In the beginning of data taking in 2011 the experimental distribution of prompt $\pi^+\pi^-$ pairs on Q_X and Q_Y were reconstructed and compared with similar simulated distributions, calculated accounting the field map of the magnet placed between the Be target and the Pt foil. In Fig. 12 the $\pi^+\pi^-$ pair distribution over Q_X for different interval of Q_Y is presented. All distributions have a maximum at $Q_x = 0$ because the vertical component of magnetic field is small. Fig. 13 shows the experimental distribution of $\pi^+\pi^-$ pairs over Q_Y and the same simulated spectrum using magnetic field map. The difference between the experimental and simulated peak position is caused by the difference between the calculated and real bending power of the magnet because of magnetic field degradation during a setup tuning before beginning of data taking.

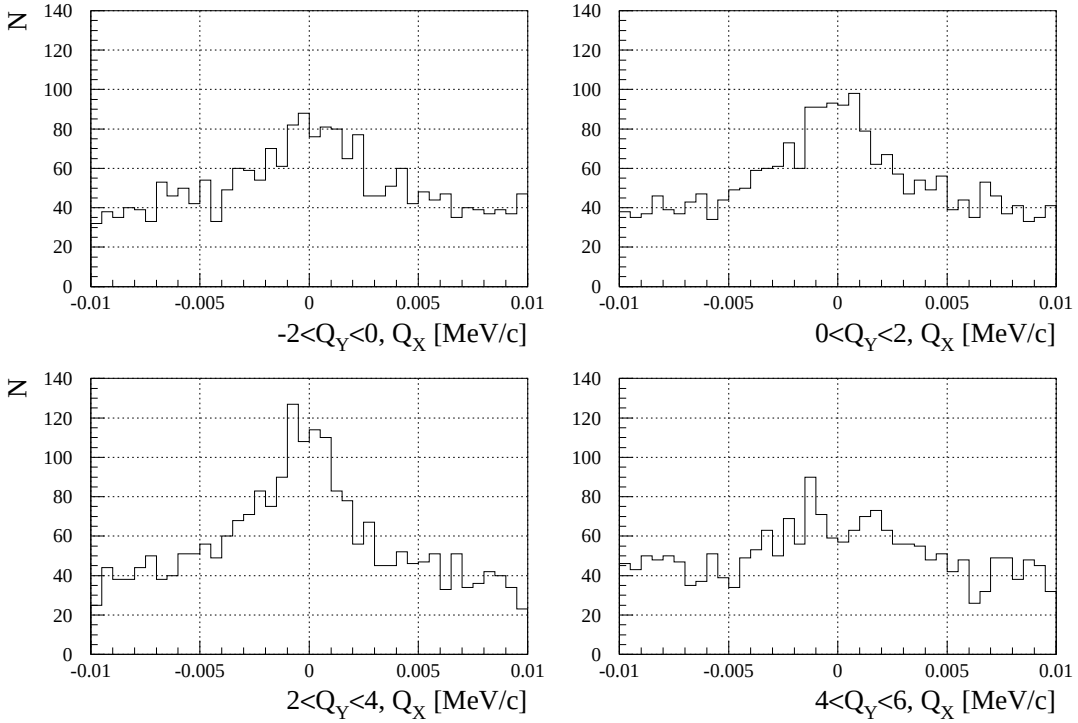

Figure 12: *Experimental distributions for $\pi^+\pi^-$ pairs over Q_X with different criteria for Q_Y. For all Q_Y intervals the Coulomb peak in Q_X are placed at zero as the vertical component of magnetic field is negligible.*

To monitor the magnetic field degradation during the 2011 run not only $\pi^+\pi^-$ pairs were used, but also e^+e^- pairs, which allow to estimate the strength of the magnetic field with a better accuracy. Fig. 14 presents the e^+e^- pair distributions over Q_X for 4 data sets collected in June-August 2011 run and demonstrates their stability. The same distributions over Q_Y are presented in Fig. 15. The peak at $Q_Y = 0$ is assigned to the e^+e^- pairs generated after the magnet, the second (non-zero Q_Y) peak is associated mainly with Dalitz pairs from the Be target. Therefore, the second peak position allows to estimate the magnetic field strength degradation during the 2011 run. Using Q_Y distribution of e^+e^- pairs the dependence of magnetic field strength (MFS) on time during run 2011 was extracted as presented in Fig.16. At the beginning of run the MFS decrease was strong but later the magnet degradation rate was much less. The total decrease in the magnet bending power during 2011 was about 2 times. That leads to a significant increase of the background and thus the long-lived $A_{2\pi}$ can not be observed with required accuracy.

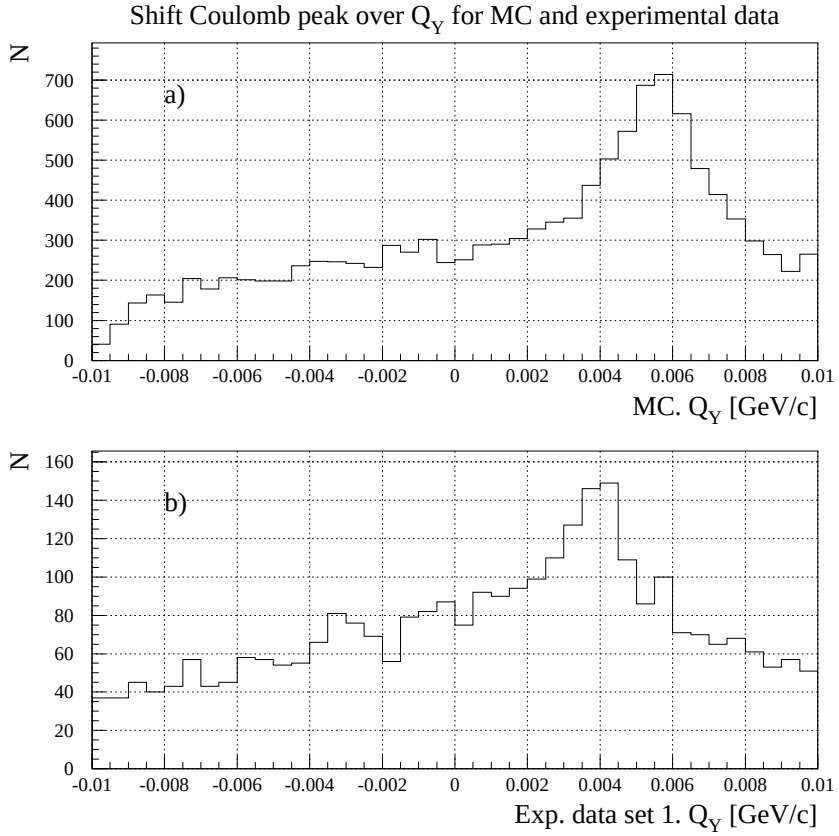

Figure 13: *The Coulomb peak of $\pi^+\pi^-$ pairs over Q_Y for: a) MC simulation; b) experimental data collected in the period from 25/06/2011 to 01/07/2011. The difference in the peak position illustrates the difference between the calculated and real bending power of the magnet.*

The most reasonable cause of the magnet degradation can be an irradiation of the magnet poles by secondary particles. In dedicated literatures the irradiation by neutrons is named most often as the reason of decrease in magnetization of permanent magnet. The products of neutron-nucleus interactions generate a local matter heat above the Curie temperature, changing the domain orientation and decreasing the magnetic field strength [34]. The greatest influence on the MFS is caused by the neutrons with energy of 1 MeV and higher (Fig.17). The influence of low energy reactor neutrons on magnetization is smaller than above (Fig.18). The estimation of fluxes of high energy neutrons and other particles through the magnet poles are shown in Table 8; this total particle flux in 2011 was equal $2.5 \cdot 10^{10}$ cm^{-2}. From this table we can conclude that the exited Be nuclei which are produced by the primary proton beam interaction with Be target are the main source of neutrons: the total flux of neutrons with energy of 1 MeV and higher through the magnet poles in the run 2011 is $3.2 \cdot 10^{12}$/cm^{-2}. The energy interval of neutrons from exited Be nuclei is qualitatively similar to the one of spallation sources. The influence of neutron flux of spallation sources on magnetic field strength is shown in Fig.17. We conclude that the neutron flux at the level of $3 \cdot 10^{12}$cm^{-2} can reduce the pole magnetization.

Few times during data taking the magnet had been unsupervised irradiated when a control over the beam extraction was lost because of different accident. In this case the protons can interact with the magnet directly or with other massive parts of target station and generate the intensive flux of neutrons and other particles through the poles. The difference in Q_Y distributions of e^+e^- pairs collected just before and after the accident confirm the decrease of MFS in such cases.

Table 8: *Maximal estimation of π, p, n, γ flux due to nuclear interaction of 24 GeV protons with Be target.*

Fluxs of high energy particles	
$\pi^+ \& \pi^-$	10^4 spill^{-1}cm^{-2}
p	$0.23 \cdot 10^4$ spill^{-1}cm^{-2}
n	$0.23 \cdot 10^4$ spill^{-1}cm^{-2}
γ	10^4 spill^{-1}cm^{-2}
Total per run	$2.5 \cdot 10^{10}$ cm^{-2}
Neutron evaporation from the Be target	
Total per run	$3.2 \cdot 10^{12}$ cm^{-2}

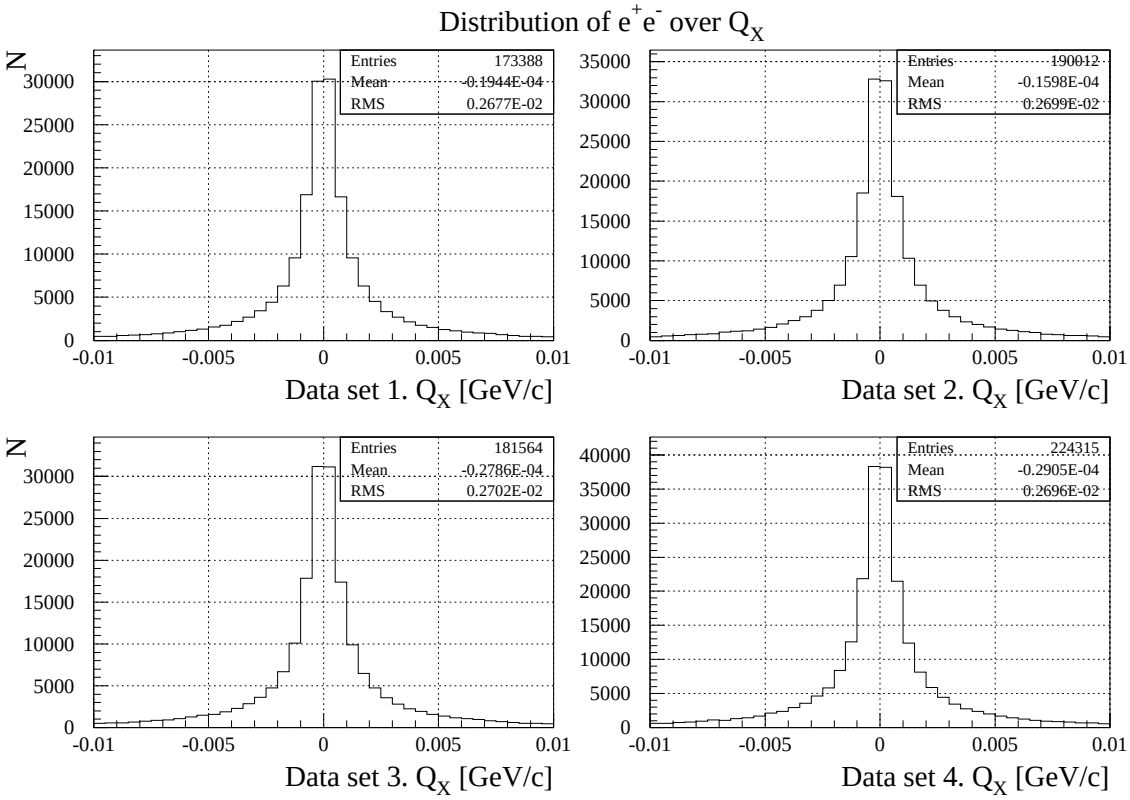

Figure 14: *e^+e^- pair distributions over Q_X for 4 time intervals: data set 1 — from 25/06/2011 to 01/07/2011; data set 2 — from 22/07/2011 to 31/07/2011; data set 3 — from 04/08/2011 to 09/08/2011; data set 4 — from 24/08/2011 to 28/08/2011.*

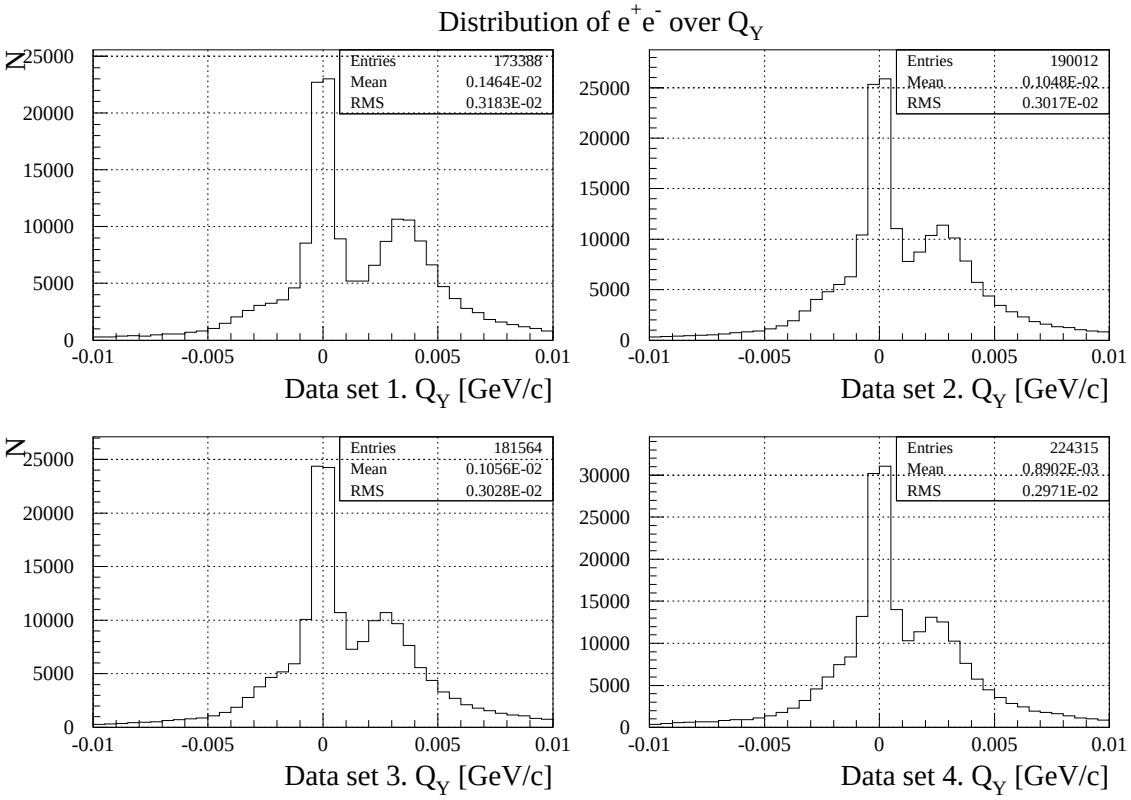

Figure 15: *e^+e^- pair distributions over Q_Y. for 4 time intervals: data set 1 — from 25/06/2011 to 01/07/2011; data set 2 — from 22/07/2011 to 31/07/2011; data set 3 — from 04/08/2011 to 09/08/2011; data set 4 — from 24/08/2011 to 28/08/2011. Changing in position of the peak at non-zero Q_Y illustrates the permanent magnet degradation.*

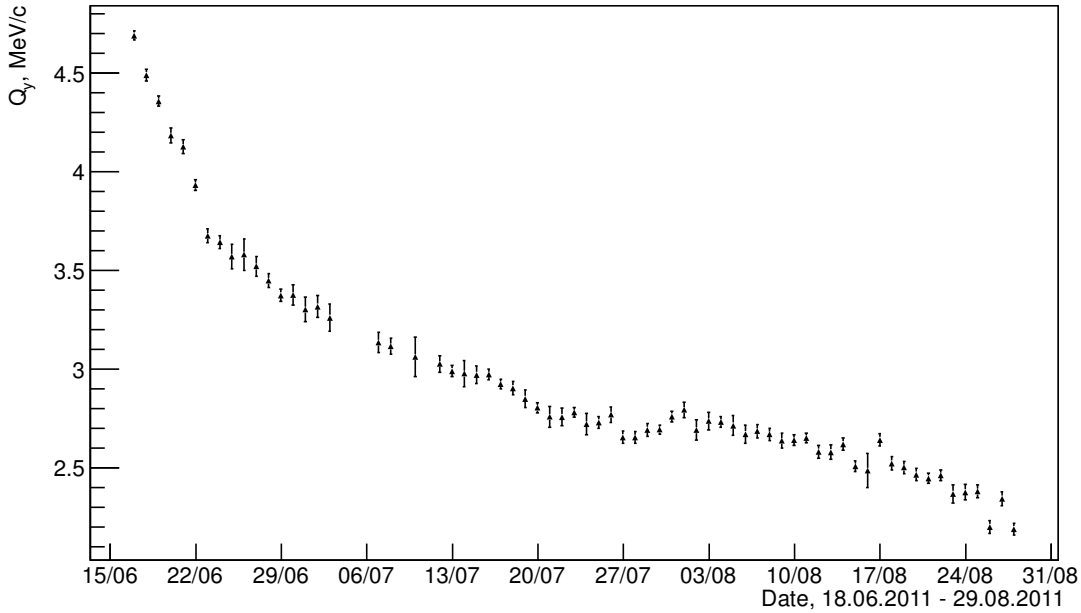

Figure 16: *The position of second peak in Q_Y distributions of e^+e^- pairs (see Fig.15) versus dates.*

9 Magnet for data taking in 2012

The degradation of the permanent magnet, made of $Ne_2Fe_{14}B$, during 2011 requires its replacement for reaching the desirable accuracy in observation of long-lived $A_{2\pi}$. An alternative with the electromagnet has been considered [35] and excluded mainly because of the large weight of 64 kg and resulting problems with its installation inside the existing target station.

A new permanent magnet with poles made of SmCo will be produced for the 2012 run. The main reason is the strong resistivity of SmCo to the neutron irradiation. The Curie temperature of this material is about $700^0 C$ and more than two times higher than the one of $Ne_2Fe_{14}B$. One can see (Fig.17) that a magnetization reduction of 2 occurs at neutron flux of $5{\cdot}10^{14} \div 5{\cdot}10^{16}$ for Nd magnet and at $5 \cdot 10^{19}$ for Sm magnet. The strong radiation resistivity of Sm magnets is confirmed by the reactor neutron measurements (Fig.18) and by measurements using neutrons produced by 86 MeV proton beam (Fig.19). The sketches of the magnet are shown in Fig.20. The dependence of magnetic field strength on Z (along the secondary beam axis) is shown in Fig.21. The magnetic field in its center is equal to 0.3 T (0.13 T for the previous magnet), the value of $B_X \cdot L = 0.023$ Tm (0.01 Tm for the previous one). The Q_Y distribution of Coulomb pairs for this magnet is shown in Fig.9.

The more that twice higher bending power of the new magnet will provide a low enough background even in a case of its significant degradation. A new design of the magnet installation device allows to replace the magnet quickly in a case of its crucial degradation due to an unsupervised irradiation at accidents with the primary beam control system. Thus the DIRAC setup with the new magnet will allow to justify the existence of the long-lived states of $A_{2\pi}$.

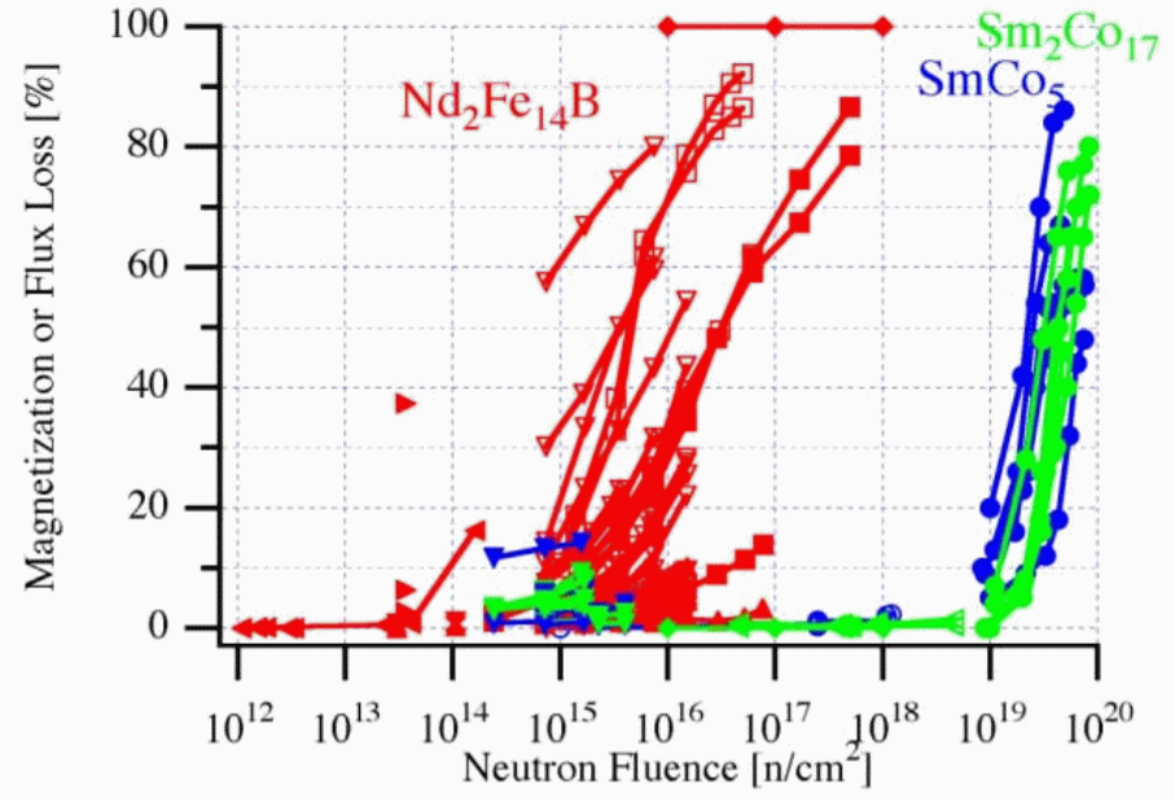

Figure 17: *Summary on the magnetization loss in % versus the neutron fluxes per cm^2 for Nd-Fe-B and Sm-Co magnets [32]. The Nd-Fe-B magnets (red lines) have been irradiated by 65 MeV neutrons. The Sm-Co magnets (blue and green lines) have been irradiated by spallation sources with a high energy tail but a peak at low energy (1~15 MeV).*

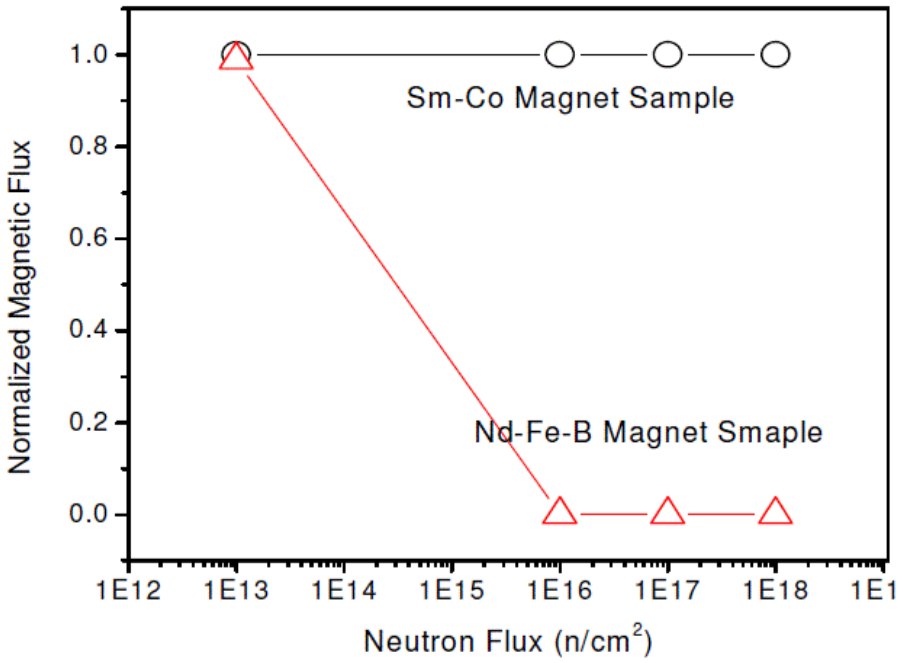

Figure 18: *Normalized magnetization of Nd-Fe-B and Sm-Co magnets versus the reactor neutron flux [31].*

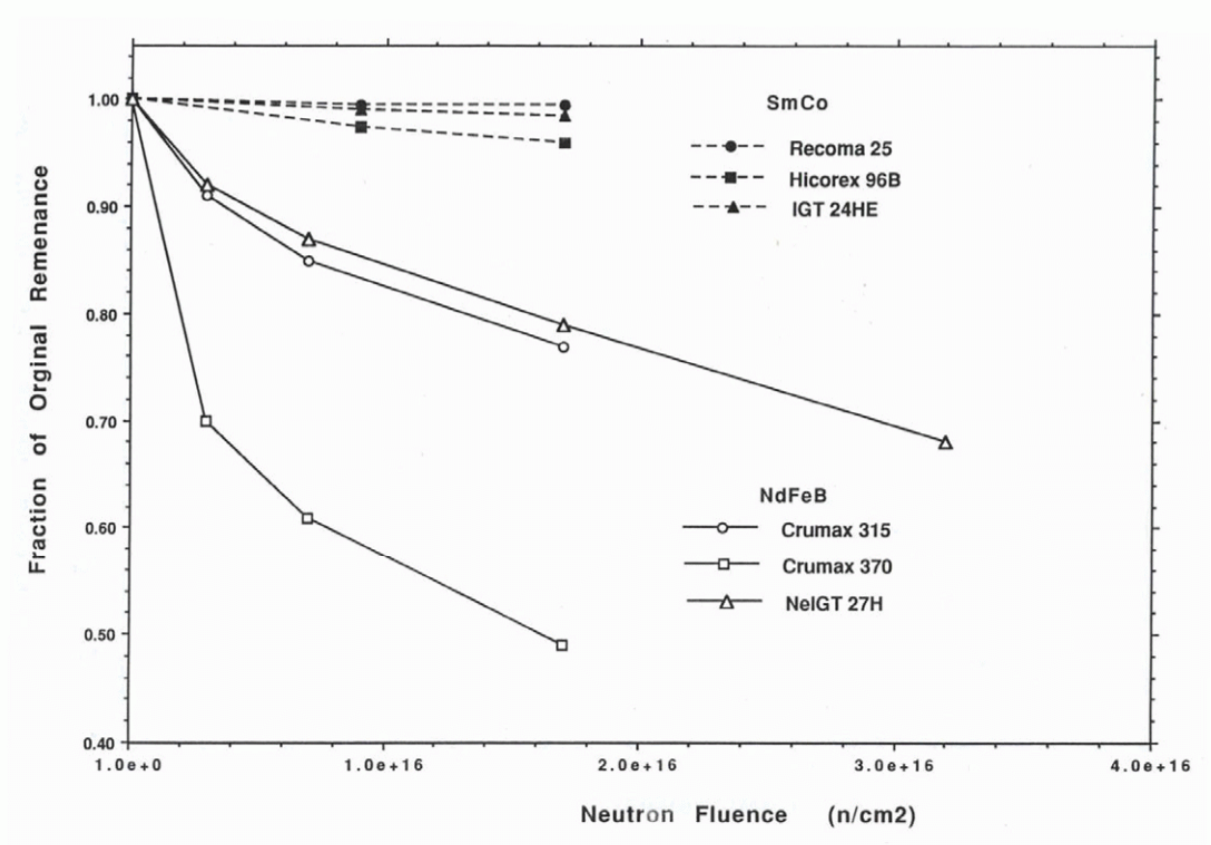

Figure 19: *Normalized magnetization of Nd-Fe-B and Sm-Co magnets versus fluxes of the neutron produced by a high-intensity proton beam of 86 MeV [33].*

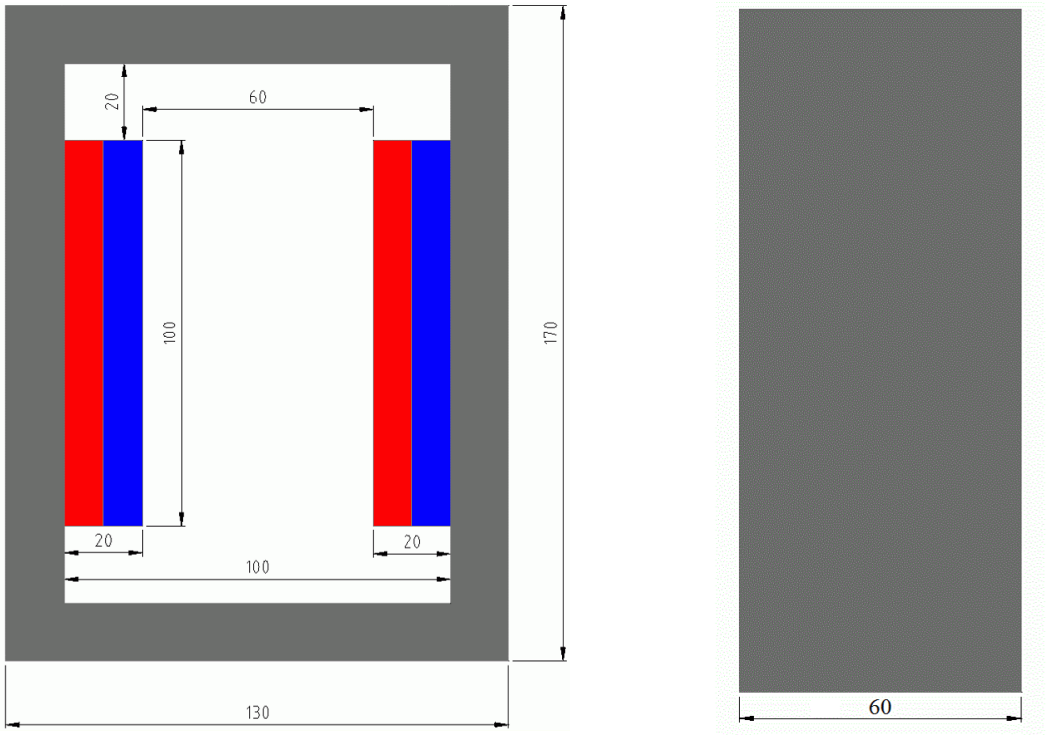

Figure 20: *The sketches of the new magnet (front view in left and side view in right).*

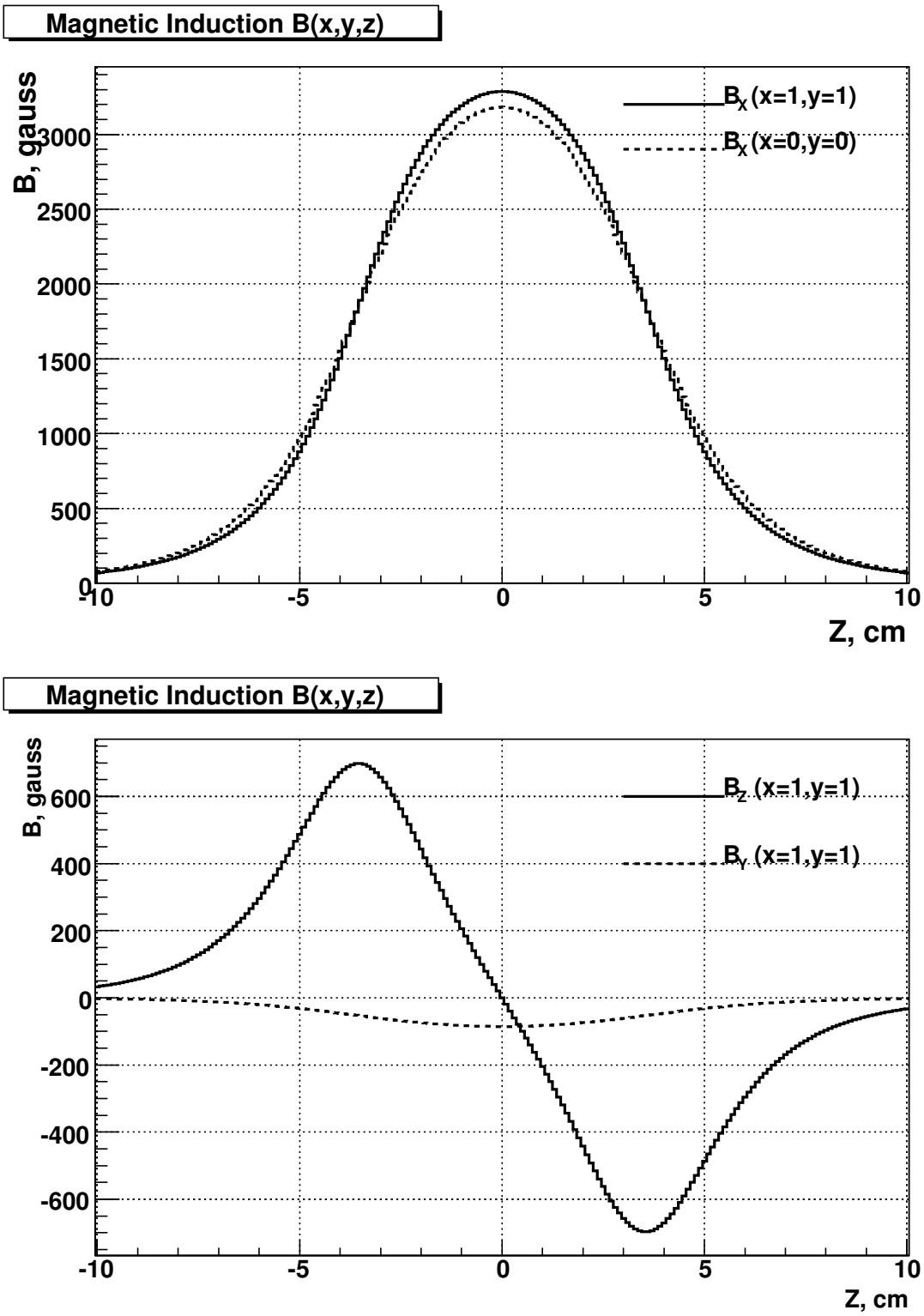

Figure 21: *Calculated values of different components of magnetic field strength of the new magnet.*

10 Measurement of multiple scattering for different materials

In the last DIRAC result (9) [1] the statistical and systematic errors in the value of $|a_0 - a_2|$ are of the order of 3%. With the additional data collected in 2008–2010 the statistical error is expected to be reduced to 2%. So some extra steps should be taken for reducing the systematic error also.

The current value of the systematic error by 80% is determined by the accuracy of multiple scattering estimation in the Ni target. The angle of multiple scattering in the Ni target was measured during two months in 2003 in parallel with the ordinary data taking [12]. The accuracy of this measurement is 1% and mainly determined by the amount of collected data. So repetition of this measurement with a higher statistics is required.

Moreover, now the data acquisition system allows to collect events at 5 times higher rate compared to 2003. So influence of statistics on the accuracy of the scattering angle measurement can be decreased significantly. The measurement procedure allows to install few scatterers in parallel. It will permit to estimate systematic error in the angle measurement with scatterer of the same material and to perform measurement with different materials. It is planed to install as the scatterer the Ni target of 100 μm used in 2003–2010 to measure the scattering angle of the specific object. In addition few pieces of Nickel, Beryllium and Platinum foils will be installed.

During 6 months in 2011, in parallel with the ordinary data taking, the data for measuring the multiple scattering angles in 9 scatterers were collected. In 2012 this measurements will be continued.

11 Conclusion

The 2010 and 2011 data analysis shows that the long-lived states of $\pi^+\pi^-$ atoms can be observed with the existing DIRAC setup at the level larger than 9σ during 6 months run in 2012 with the total spill number of 10^6 and the correspondent total proton flux through the target of $3 \cdot 10^{17}$. The new permanent magnet with poles made of SmCo will keep the background at the low level.

References

[1] B. Adeva *et al.*, Physics Letters B 704 (2011) 24.

[2] B. Adeva *et al.*, Phys. Lett. B 619 (2005) 50.

[3] L. G. Afanasyev, "Observation of $\pi^+\pi^-$ atom", PhD thesis, JINR, Dubna, 1997.

[4] L. Afanasyev, G. Colangelo, J. Schacher, HadAtom05 — Workshop on Hadronic Atoms, February 15–16, 2005, Bern, Switzerland, http://arxiv.org/abs/hep-ph/0508193.

[5] G.J.M.Austen, J.J. de Swart, Phys.Rev.Lett. 50 (1983) 2039.

[6] S.M. Bilenky *et al.*, Yad. Phys. 10 (1969) 812; (Sov. J. Nucl. Phys. 10 (1969) 469).

[7] P. Buettiker, S. Descotes-Genon, B. Moussallam, Eur. Phys. J. C 33 (2004) 409.

[8] G. Colangelo, J. Gasser and H. Leutwyler, Nucl. Phys. B603 (2001) 125.

[9] S. Descotes *et al.*, LPT-ORSAY/03-82, ECT*-03-06, IPNO DR 03-09; hep-ph/0311120.

[10] B. Adeva *et al.*, SPSC-P-284-ADD-5; hep-ph/1319290.

[11] S. Deser *et al.*, Phys. Rev. 96 (1954) 774.

[12] A. Dudarev, V. Kruglov, L. Kruglova, M. Nikitin, "Pion multiple Coulomb scattering in the DIRAC experiment", DIRAC NOTE 08-06, http://dirac.web.cern.ch/DIRAC/i_notes.html

[13] G.V. Efimov, M.A. Ivanov and V.E. Lyubovitskij, Yad. Fiz. 44 (1986) 460; (Sov. J. Nucl. Phys. 44 (1986) 296.

[14] G. V. Efimov, M. A. Ivanov and V. E. Lyubovitskij, Yad. Fiz. 44 (1986) 460; Sov. J. Nucl. Phys. 44 (1986) 296.

[15] D.Eiras and J.Soto, Phys.Lett. B491 (2000) 101; hep-ph/0005066.

[16] A. Gashi *et al.*, Nucl. Phys. A628 (1998) 101.

[17] J. Gasser *et al.*, Phys.Rev. D64 (2001) 016008; hep-ph/0103157.

[18] O. E. Gorchakov *et al.*, Yad. Fiz. 63 (2000) 1936; (Phys. At. Nucl. 63 (2000) 1847).

[19] M.A. Ivanov *et al.*Phys. Rev. D58 (1998) 094024.

[20] H. Jallouli and H. Sazdjian, Phys. Rev. D58 (1998) 014011; Erratum: ibid., D58 (1998) 099901.

[21] A. Karimhodjaev and R. N. Faustov, Yad. Fiz. 29 (1979) 463; Sov.J.NuclPhys. 29 (1979) 232.

[22] H. Leutwyler, Proc. XXVI Int. Conf. on High Energy Physics, Dallas, 1992, edited by J. R. Sanford, IAP Conf. Proc. N.272 (AIP New York 1993) 185.

[23] J.R. Batley *et al.*, Eur. Phys. J. C 64 (2009) 589–608.

[24] J.R. Batley *et al.*, Eur. Phys. J. C 70 (2010) 635–657.

[25] L. L. Nemenov and V. D. Ovsyannikov, Phys. Lett. B514 (2001) 247.

[26] L. L. Nemenov, V. D. Ovsyannikov and E. V. Chaplygin, Nucl. Phys. A 710 (2002) 303.

[27] L. L. Nemenov, Yad. Fiz 41 (1985) 980; Sov. J. Nucl. Phys. 41 (1985) 629.

[28] J. Schweizer, *Phys. Lett. B* 587 (2004) 33, arXiv:hep-ph/0401048;
J. Schweizer, *Eur. Phys. J. C* 36 (2004) 483. arXiv:hep-ph/0405034.

[29] J. Uretsky and J. Palfrey, Phys. Rev. 121 (1961) 1798.

[30] M.Zhabitsky, DIRAC Note 2007-11.

[31] J. Liu et al, Paper 2036, Proceedings of Space Nuclear Conference 2007, Boston, Massachusetts, June 24-28 2007.

[32] X.-M. Marchal, T. Bizen, Y. Asano, JASRI/SPring-8, Hyogo-ken, Japan, H. Kitamura, RIKEN/Spring-8 Center, Hyogo, Japan, THPCH135, Proceedings of EPAC 2006, Edinburgh, Scotland.

[33] R. Hardekopf, Technical Note September 7, 2001, SNS01-TCN-0599.

[34] THERMAL STABILITY AND RADIATION RESISTANCE OF SM-CO BASED PERMANENT MAGNETS Jinfang Liu et al, Proceedings of Space Nuclear Conference 2007, Boston, Massachusetts, June 24-28,2007
Summary of Radiation Damage Studies on Rare Earth Permanent Magnets J.T.Volk Fermilab
V.Yu.Schegolev, B.V.Florko, BRADIATION HARDNESS OF NDFEB PERMANENT MAGNETS IN HIGH-ENERGY NEUTRON FIELDS AT CYCLOTRONS. Proceedings of RuPAC XIX, Dubna,2004
X.-M.Marchal, T.Bizen, Y.Asano, 65 MEV NEUTRON IRRADIATION OF ND-FE-B PERMANENT MAGNETS JASRI/SPring-8, Hyogo-ken, Japan, H. Kitamura, RIKEN/Spring-8 Center, Hyogo, Japan, THPCH135, Proceedings of EPAC 2006, Edinburgh, Scotland
Alexander B. Temnykh, Measurement of NdFeB permanent magnets demagnetization induced by high energy electron radiation Wilson Lab, Cornell University, LEPP, Ithaca, NY 14850, USA Nuclear Instruments and Methods in Physics Research A 587 (2008) 13
Robert Hardekopf, Permanent Magnet Radiation Resistance in the SNS Linac, Los Alamos National Laboratory, SNS Technical Note September 7, 2001, SNS01 TCN 0599
J. M. Carpenter, Neutron Production, Moderation, and Characterization of Sources URL: http://www.neutron.anl.gov/NeutronProduction.pdf
A.Letourneau et al, Neutron production in bombardments of thin and thick W, Hg, Pb targets by 0.4, 0.8, 1.2, 1.8 and 2.5 GeV protons. Nuclear Instruments and Methods in Physics Research B 170 (2000) 299-322

[35] A.Vorozhtsov, Preliminary electromagnetic design and cost estimate of C-shape dipole magnet required for DIRAC experiment, DIRAC-NOTE-2011-10, http://dirac.web.cern.ch/DIRAC/note/note1110.pdf.